Pramana – J. Phys. (2022) 96:53
https://doi.org/10.1007/s12043-022-02295-1

Quantum Langevin dynamics of a charged particle in a magnetic field: Response function, position–velocity and velocity autocorrelation functions

SURAKA BHATTACHARJEE[1],*, URBASHI SATPATHI[2] and SUPURNA SINHA[1]

[1]Raman Research Institute, Bengaluru 560 080, India
[2]International Centre for Theoretical Sciences, Tata Institute of Fundamental Research, Bengaluru 560 089, India
*Corresponding author. E-mail: suraka@rri.res.in, surakabhatta@gmail.com

MS received 28 August 2021; revised 22 October 2021; accepted 25 October 2021

Abstract. We use the quantum Langevin equation as a starting point to study the response function, the position–velocity correlation function and the velocity autocorrelation function of a charged quantum Brownian particle in the presence of a magnetic field and linearly coupled to a heat bath via position coordinate. We study two bath models – the Ohmic bath model and the Drude bath model and make a detailed comparison in various time–temperature regimes. For both bath models, there is a competition between the cyclotron frequency and the viscous damping rate giving rise to a transition from an oscillatory to a monotonic behaviour as the damping rate is increased. In the zero point fluctuation dominated low-temperature regime, non-trivial noise correlations lead to some interesting features in this transition. We study the role of the memory time-scale which comes into play in the Drude model and study the effect of this additional time-scale. We discuss the experimental implications of our analysis in the context of experiments in cold ions.

Keywords. Quantum Langevin equation; response function; autocorrelation function; cyclotron frequency; memory kernel.

PACS Nos **05.40.Jc; 05.40.-a; 05.30.-d; 05.10.Gg; 42.50.Lc**

1. Introduction

The response function of a system, which measures the response of a system to an external perturbation, characterises the intrinsic properties of the system, for instance, electric polarisability, magnetic susceptibility and so on [1]. Thus, the response function of a system is of central importance in the realm of non-equilibrium statistical mechanics [2].

In recent years, there have been theoretical and experimental research on diffusion in oscillatory and damped regimes. In particular, Bloch oscillations and their damping due to spontaneous emission have been studied in the context of cold atoms in optical lattices [3,4].

In the earlier work [3,4], the researchers addressed the issue of Brownian motion of neutral particles, which signifies the erratic motion of particles suspended in a fluid, caused by the random collision of the particle with the molecules present in the viscous medium [5]. On the contrary, here we consider the motion of a charged particle in the presence of a magnetic field in a viscous environment. Moreover, there has been a study of the classical Langevin dynamics of a charged particle in a magnetic field in the high-temperature classical domain [6].

In contrast, in this paper we focus on analysing the position response function of a charged particle in a viscous environment in the presence of a magnetic field using the quantum Langevin equation (QLE). The system under consideration is characterised by two competing rates: the cyclotron frequency $\omega_c = qB/mc$, where m is the mass of the particle, q is the charge, c is the speed of light, B is the strength of the magnetic field and γ is the rate associated with dissipation. Dattagupta and Singh [7] analysed such a system. However, we go beyond that study and explore various time regimes and analyse in detail the onset

Published online: 03 March 2022

of oscillatory response of this system for two different bath models – the Ohmic bath and the Drude bath models. In the Drude bath model, there is an additional time-scale, the memory time τ which introduces some interesting quantitative effects. We also study the behaviour of the position–velocity correlation function and the velocity autocorrelation function in various time–temperature regimes for the two bath models.

The paper is organised as follows. In §2 we introduce the quantum Langevin equation and define the response function, the position–velocity correlation function and the velocity autocorrelation function. In §3 we analyse the position response function for the Ohmic model and the Drude model. In §4 we analyse the position–velocity correlation function for the two models and in §5 we analyse the velocity autocorrelation function for the system for the two bath models. In §6 we discuss the results of our study and compare the behaviour of the response function, the position–velocity correlation function and the velocity autocorrelation function for the two bath models at various time–temperature regimes. In §7 we discuss the experimental implications of our study and finally in §8 we end the paper with some concluding remarks.

2. Position correlation function in the presence of a magnetic field

The Hamiltonian for the motion of a charged quantum Brownian particle in the presence of a magnetic field and linearly coupled via position coordinate to a passive heat bath, characterised by the bath in thermal equilibrium is given by [8,9]

$$H = \frac{1}{2m}\left(p - \frac{qA}{c}\right)^2 + \sum_j \left[\frac{p_j^2}{2m_j} + \frac{1}{2}m_j\omega_j^2\left(q_j - r\right)^2\right]. \tag{1}$$

where m, q, r, p are the mass, charge, position and momentum of the particle respectively, whereas m_j, q_j, p_j and ω_j are the mass, position coordinate, momentum coordinate and frequency of the jth oscillator in the bath respectively. $A(r)$ represents the vector potential corresponding to the applied magnetic field. We derive the QLE for this system. Below we outline the basic steps used in the derivation of the QLE: (i) We first obtain the Heisenberg equations of motion for the heat bath and the system of the charged particle linearly coupled to the heat bath via position coordinate. We then solve these equations for the bath variables, and substitute the solution into the equations for the charged particle to obtain a reduced description of the particle motion. The solution contains explicit expressions for the dynamical variables at time t in terms of their initial values. (ii) We make specific assumptions about the initial state of the system. For instance, we assume that the heat bath was at thermal equilibrium, which is satisfied by the Fourier transform of the memory function being a positive real function [8]. Thus, the generalised QLE is formulated from the Hamiltonian (eq. (1)), where the effect of the passive heat bath is only retained in the memory kernel and the random fluctuating force [8,10–12]:

$$m\ddot{\vec{r}}(t) = -\int \mu(t-t')\dot{\vec{r}}(t')\mathrm{d}t' + \frac{q}{c}(\dot{\vec{r}}(t)\times\vec{B}) + \vec{F}(t), \tag{2}$$

where $\mu(t)$ is the memory kernel and $\vec{F}(t)$ is the random force having the following properties [8,12]:

$$\langle F_\alpha(t)\rangle = 0 \tag{3}$$

$$\frac{1}{2}\langle\{F_\alpha(t), F_\beta(0)\}\rangle = \frac{\delta_{\alpha\beta}}{2\pi}\int_{-\infty}^{\infty}\mathrm{d}\omega\mathrm{Re}[\mu(\omega)]\hbar\omega\coth\left(\frac{\hbar\omega}{2k_BT}\right)\mathrm{e}^{-i\omega t} \tag{4}$$

$$\langle[F_\alpha(t), F_\beta(0)]\rangle = \frac{\delta_{\alpha\beta}}{\pi}\int_{-\infty}^{\infty}\mathrm{d}\omega\mathrm{Re}\mu(\omega)]\hbar\omega\mathrm{e}^{-i\omega t}. \tag{5}$$

Here $\alpha, \beta = x, y, z$ and $\delta_{\alpha\beta}$ is the Kronecker delta function. Also $\mu(\omega) = \int_{-\infty}^{\infty}\mathrm{d}t\,\mu(t)\mathrm{e}^{i\omega t}$.

We consider a uniform magnetic field along the z-axis. This results in the following solutions to the motion of the charged particle in the x–y plane [12]:

$$\tilde{x}(\omega) = \frac{1}{m}\frac{i\omega_c\tilde{F}_y(\omega) - (\omega - iK(\omega))\tilde{F}_x(\omega)}{\omega[\omega^2 - \omega_c^2 - \tilde{K}(\omega)^2 - 2i\omega\tilde{K}(\omega)]} \tag{6}$$

$$\tilde{y}(\omega) = \frac{1}{m}\frac{-i\omega_c\tilde{F}_x(\omega) - (\omega - iK(\omega))F_y(\omega)}{\omega[\omega^2 - \omega_c^2 - \tilde{K}(\omega)^2 - 2i\omega\tilde{K}(\omega)]}. \tag{7}$$

Here, $\omega_c = (eB/mc)$ is the cyclotron frequency, $K(\omega) = (\mu(\omega)/m)$. Using properties of the random force [13], we can write the position autocorrelation function for the x, y components [12],

$$C_x(t) = \frac{1}{2}\langle\{x(t), x(0)\}\rangle = \frac{\hbar}{2\pi}\int_{-\infty}^{\infty} \mathrm{d}\omega \mathrm{Re}[K(\omega)] \times \frac{\left[(\omega + \mathrm{Im}[K(\omega)])^2 + \omega_c^2 + \mathrm{Re}[K(\omega)]^2\right] \coth\left(\frac{\hbar\omega}{2k_BT}\right) \mathrm{e}^{-i\omega t}}{m\omega\left\{\left[(\omega + \mathrm{Im}[K(\omega)])^2 + \omega_c^2 + \mathrm{Re}[K(\omega)]^2\right]^2 - 4\omega_c^2\,(\omega + \mathrm{Im}[K(\omega)])^2\right\}}. \tag{8}$$

The same expression is obtained for the y component $C_y(t) = \frac{1}{2}\langle\{y(t), y(0)\}\rangle$. Using the position autocorrelation function one can get various physical observables such as the mean square displacement, response function, position–velocity correlation function and velocity autocorrelation function. In ref. [12], the mean square displacement has been analysed in detail. In the following subsections, we shall discuss the expressions for the response function, position–velocity correlation function and velocity autocorrelation function, all evaluated using the position correlation function (defined in eq. (8)) as a starting point. We analyse the behaviour of these observables in various time–temperature regimes for two bath models – the Ohmic model and the Drude model.

2.1 *Response function*

The response function pertaining to an external perturbation $f(t)$ is given by

$$\langle x(t)\rangle = \int R(t - t')f(t')\mathrm{d}t'. \tag{9}$$

In the Fourier domain, the response function $R_x(\omega)$ can be expressed in terms of the position correlation function $\mathrm{C}_x(\omega)$ as follows [1,14]:

$$\mathrm{Im}R_x(\omega) = \frac{1}{\hbar}\tanh\left(\frac{\hbar\omega}{2k_BT}\right) C_x(\omega). \tag{10}$$

From eq. (8), we get

$$C_x(\omega) = \frac{\hbar}{m}\mathrm{Re}[K(\omega)] \frac{\left[(\omega + \mathrm{Im}[K(\omega)])^2 + \omega_c^2 + \mathrm{Re}[K(\omega)]^2\right] \coth\left(\frac{\hbar\omega}{2k_BT}\right)}{\omega\left\{\left[(\omega + \mathrm{Im}[K(\omega)])^2 + \omega_c^2 + \mathrm{Re}[K(\omega)]^2\right]^2 - 4\omega_c^2\,(\omega + \mathrm{Im}[K(\omega)])^2\right\}}. \tag{11}$$

Using eqs (10) and (11), we get

$$\mathrm{Im}\,R_x(\omega) = \frac{1}{m}\mathrm{Re}[K(\omega)] \frac{\left[(\omega + \mathrm{Im}[K(\omega)])^2 + \omega_c^2 + \mathrm{Re}[K(\omega)]^2\right]}{\omega\{[(\omega + \mathrm{Im}[K(\omega)])^2 + \omega_c^2 + \mathrm{Re}[K(\omega)]^2]^2 - 4\omega_c^2(\omega + \mathrm{Im}[K(\omega)])^2\}}. \tag{12}$$

Knowing $\mathrm{Im}R_x(\omega)$, one can get the expression for $\mathrm{Re}R_x(\omega)$ using the Kramers Kronig relation [15]

$$\mathrm{Re}R_x(\omega) = \frac{1}{\pi}P\int_{-\infty}^{\infty} \frac{\omega'\,\mathrm{Im}\,R_x(\omega')}{(\omega'^2 - \omega^2)}\mathrm{d}\omega', \tag{13}$$

where P refers to the principal value of the integral.

Collecting the real and imaginary parts we get, $R_x(\omega) = \mathrm{Re}\,R_x(\omega) + i\,\mathrm{Im}\,R_x(\omega)$, the Fourier transform of which gives the time-dependent position response function $R_x(t)$,

$$R_x(t) = \frac{1}{2\pi}\int_{-\infty}^{\infty} R_x(\omega)\mathrm{e}^{-i\omega t} = \mathcal{F}[R_x(\omega)] = \mathcal{F}[\mathrm{Re}\,R_x(\omega)] + i\mathcal{F}[\mathrm{Im}\,R_x(\omega)]. \tag{14}$$

2.2 *Position–velocity correlation function*

The position–velocity correlation function is defined as

$$C_{xv_x}(t) = \frac{1}{2}\langle\{x(t), v_x(0)\}\rangle = \frac{1}{2}\langle\{x(0), v_x(-t)\}\rangle = \frac{\mathrm{d}}{\mathrm{d}t}\frac{1}{2}\langle\{x(t), x(0)\}\rangle = \frac{\mathrm{d}}{\mathrm{d}t}C_x(t). \tag{15}$$

Using eq. (8), we get

$$C_{xv_x}(t) = \frac{-i\hbar}{2\pi m}\int_{-\infty}^{\infty} \mathrm{d}\omega\,\mathrm{Re}[K(\omega)] \frac{[(\omega + \mathrm{Im}[K(\omega)])^2 + \omega_c^2 + \mathrm{Re}[K(\omega)]^2]\coth(\frac{\hbar\omega}{2k_BT})\mathrm{e}^{-i\omega t}}{\{[(\omega + \mathrm{Im}[K(\omega)])^2 + \omega_c^2 + \mathrm{Re}[K(\omega)]^2]^2 - 4\omega_c^2(\omega + \mathrm{Im}[K(\omega)])^2\}}. \tag{16}$$

2.3 *Velocity autocorrelation function*

The velocity autocorrelation function is defined as

$$C_{v_x}(t) = \frac{1}{2}\langle\{v_x(t), v_x(0)\}\rangle = -\frac{\mathrm{d}^2}{\mathrm{d}t^2}C_x(t) \tag{17}$$

$$C_{v_x}(t) = \frac{\hbar}{2\pi m}\int_{-\infty}^{\infty}\mathrm{d}\omega\,\omega\,\mathrm{Re}[K(\omega)]\frac{[(\omega+\mathrm{Im}[K(\omega)])^2+\omega_c^2+\mathrm{Re}[K(\omega)]^2]\coth(\frac{\hbar\omega}{2k_BT})\mathrm{e}^{-i\omega t}}{\{[(\omega+\mathrm{Im}[K(\omega)])^2+\omega_c^2+\mathrm{Re}[K(\omega)]^2]^2-4\omega_c^2(\omega+\mathrm{Im}[K(\omega)])^2\}}. \tag{18}$$

Since the expression for the y component position autocorrelation function is the same as that for the x component, we get the same expressions for all the physical observables corresponding to the y component as well. Note that the expressions for the response function, position–velocity correlation function and velocity autocorrelation function are valid for any memory kernel $K(t)$. In the next section, we use specific models for the memory kernel and analyse the forms of the response function, position–velocity correlation function and velocity autocorrelation function for each case. The models we analyse are [16]

1. The Ohmic model : $K(t) = 2\gamma\delta(t)$
2. The Drude model : $K(t) = \frac{\gamma}{\tau}\mathrm{e}^{-t/\tau}$.

The Ohmic model corresponds to a memory less or Markovian bath while the Drude model corresponds to an exponentially decaying memory (τ is the memory time) and is non-Markovian. Here, γ is the decay rate associated with dissipation, as mentioned in the previous section.

3. The response function

3.1 *Ohmic model*

In this case, the memory kernel is given by $K(\omega) = \gamma$, hence the imaginary part of the response function (eq. (12)) is given by

$$\mathrm{Im}\,R_x(\omega) = \frac{\gamma}{m}\frac{(\omega^2+\omega_c^2+\gamma^2)}{\omega\left[(\omega^2+\omega_c^2+\gamma^2)^2-4\omega^2\omega_c^2\right]}. \tag{19}$$

The real part $\mathrm{Re}\,R_x(\omega)$ can be obtained using the Kramers Kronig relation (eq. (13)),

$$\mathrm{Re}\,R_x(\omega) = \frac{\gamma}{m\pi}\int_{-\infty}^{\infty}\frac{\mathrm{d}\omega'}{(\omega'^2-\omega^2)} \times\frac{(\omega'^2+\omega_c^2+\gamma^2)}{[(\omega'^2+\omega_c^2+\gamma^2)^2-4\omega'^2\omega_c^2]}. \tag{20}$$

Using Cauchy's residue theorem, the above integral can be solved and is given by

$$\mathrm{Re}\,R_x(\omega) = -\frac{1}{m}\left[\frac{-\omega_c^2+\omega^2+\gamma^2}{(\omega^2+\omega_c^2+\gamma^2)^2-4\omega^2\omega_c^2}\right]. \tag{21}$$

The Fourier transforms of eqs (19) and (21) give

$$\mathcal{F}(\mathrm{Im}\,R_x(\omega)) = \frac{-i\mathrm{e}^{-\gamma t}}{2m}\left[\frac{\omega_c\sin(\omega_c t)-\gamma\cos(\omega_c t)}{\omega_c^2+\gamma^2}\right] -\frac{i}{m}\left[\frac{\gamma}{\omega_c^2+\gamma^2}\right] \tag{22}$$

$$\mathcal{F}(\mathrm{Re}\,R_x(\omega)) = \frac{\mathrm{e}^{-\gamma t}}{2m}\left[\frac{\omega_c\sin(\omega_c t)-\gamma\cos(\omega_c t)}{\omega_c^2+\gamma^2}\right]. \tag{23}$$

Here it can be noticed that the memory kernel satisfies causality, $K(t) = 0, t < 0$, which implies that the integrands appearing in the Fourier transforms are analytic in the upper half plane and can have poles only in the lower half plane.

The poles lying in the lower half plane for the Ohmic case are: $\omega = \pm\omega_c - i\gamma$. Equations (22) and (23) are given by $(-2\pi i)$ times the sum of the residues at the respective poles. Combining the above using eq. (14), we get

$$R_x(t) = \left[\frac{\gamma-\mathrm{e}^{-\gamma t}\left(\gamma\cos(\omega_c t)-\omega_c\sin(\omega_c t)\right)}{m(\omega_c^2+\gamma^2)}\right]. \tag{24}$$

In the absence of the magnetic field, for $\omega_c \to 0$, we get the expected response function of a particle coupled to an Ohmic bath [17], which is

$$R_x(t) = \frac{1}{m}\left[\frac{1-\mathrm{e}^{-\gamma t}}{\gamma}\right]. \tag{25}$$

3.2 *Drude model*

In this case, the memory kernel in the frequency domain is given by

$$K(\omega) = \frac{\gamma}{1+\omega^2\tau^2} + i\frac{\omega\gamma\tau}{1+\omega^2\tau^2}. \tag{26}$$

Here τ is the memory time. Note that for $\tau \to 0$, the Drude model kernel gives the same expression as the Ohmic model kernel.

$$\text{Re}\, K(\omega) = \frac{\gamma}{1+\omega^2\tau^2}\ ,\ \text{Im}\, K(\omega) = \frac{\omega\gamma\tau}{1+\omega^2\tau^2}. \quad (27)$$

Following steps similar to the ones used in the case of the Ohmic model, we substitute Re $K(\omega)$ and Im $K(\omega)$ in eq. (12) and obtain the response function for the Drude model. The relevant integrals pertaining to the response function have been solved numerically since the expressions involved are cumbersome and thus cannot be solved analytically.

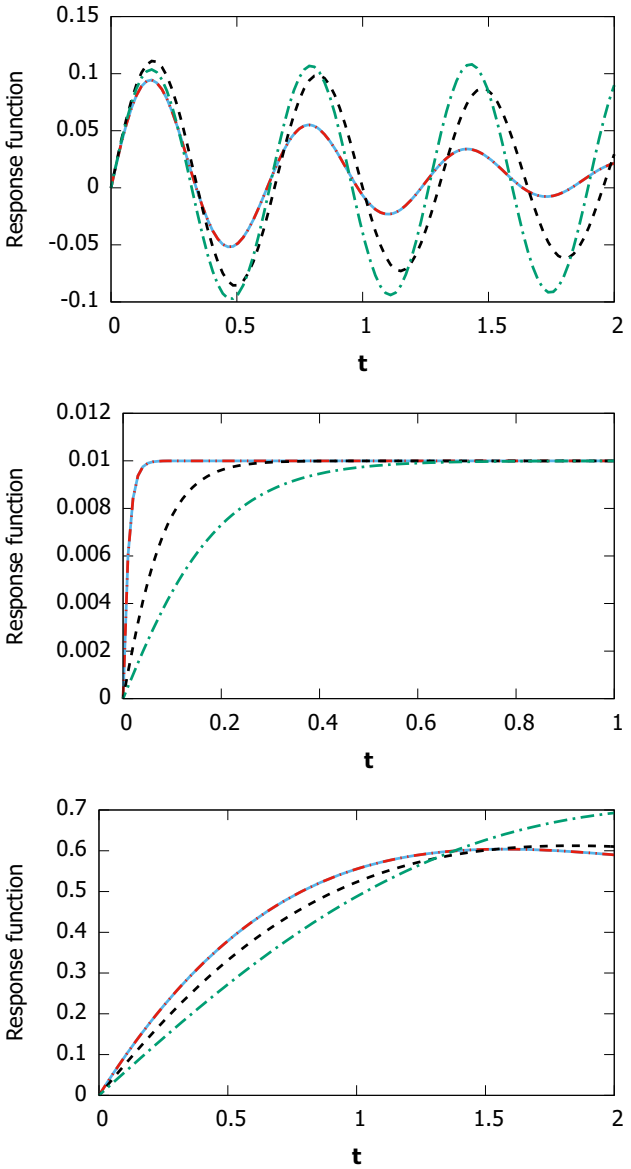

Figure 1. Time evolution of the response function. (**Top**) The underdamped ($\omega_c = 10$, $\gamma = 1$), (**middle**) the overdamped ($\omega_c = 1$, $\gamma = 100$) and (**bottom**) the critically damped ($\omega_c = 1$, $\gamma = 1$) cases. For all the cases, the solid blue line is for the Ohmic case using eq. (24), the double dot-dash red line is for the Drude case $\tau = 0$, the dashed black line is for $\tau = 0.5$ and the dot-dash green line is for $\tau = 1$.

We now explore the roles of various frequencies: the cyclotron frequency ω_c and the damping rate γ. In this context, we studied three different regimes: (i) Underdamped ($\omega_c \gg \gamma$), (ii) overdamped ($\omega_c \ll \gamma$) and (iii) critically damped ($\omega_c \sim \gamma$).

Figure 1 shows the time evolution of the response function for both the Ohmic and Drude models. For the Drude model, there is an additional time-scale, the memory time τ which comes into play. We have checked the time evolution for various τ values and noticed that the presence of τ affects the quantitative features of the response function.

4. Position–velocity correlation function

4.1 *Ohmic model*

The position–velocity correlation for the Ohmic model is given by

$$C_{xv_x}(t) = \frac{-i\gamma\hbar}{2\pi m} \times \int_{-\infty}^{\infty} d\omega \frac{(\omega^2+\omega_c^2+\gamma^2)\coth\left(\frac{\omega}{\Omega_{\text{th}}}\right) e^{-i\omega t}}{[(\omega^2+\omega_c^2+\gamma^2)^2 - 4\omega^2\omega_c^2]}, \quad (28)$$

where $\Omega_{\text{th}} = 2k_BT/\hbar$ is the thermal frequency. Using Cauchy's residue theorem, and choosing the lower contour consistent with causality, one can solve the above integral. The poles lying in the lower contour are $\omega = \pm\omega_c - i\gamma$ and $\omega = -in\pi\Omega_{\text{th}}$, where $n = 1, 2, ...\infty$. Here the additional poles at $\omega = -in\pi\Omega_{\text{th}}$ pertain to the coth term. Summing over the residues, the integration yields the result

$$\begin{aligned} C_{xv_x}(t) = -\frac{\hbar e^{-\pi t\Omega_{\text{th}}}}{4\pi m}\Bigg[&\Phi\left(e^{-\pi t\Omega_{\text{th}}}, 1, 1+\frac{-i\omega_c+\gamma}{\pi\Omega_{\text{th}}}\right) \\ &+ \Phi\left(e^{-\pi t\Omega_{\text{th}}}, 1, 1+\frac{i\omega_c+\gamma}{\pi\Omega_{\text{th}}}\right) \\ &- \Phi\left(e^{-\pi t\Omega_{\text{th}}}, 1, 1+\frac{-i\omega_c-\gamma}{\pi\Omega_{\text{th}}}\right) \\ &- \Phi\left(e^{-\pi t\Omega_{\text{th}}}, 1, 1+\frac{i\omega_c-\gamma}{\pi\Omega_{\text{th}}}\right)\Bigg] - \frac{i\hbar}{4m}e^{-\gamma t} \\ &\times\left[-\coth\left(\frac{\omega_c+i\gamma}{\Omega_{\text{th}}}\right)e^{i\omega_c t} + \coth\left(\frac{\omega_c-i\gamma}{\Omega_{\text{th}}}\right)e^{-i\omega_c t}\right], \end{aligned} \quad (29)$$

where Φ is the Hurwitz–Lerch transcendent function, defined as

$$\Phi(z, s, \alpha) = \sum_{j=0}^{\infty} \frac{z^j}{(j+\alpha)^s}. \tag{30}$$

In contrast to the response function, the position–velocity correlation function has a temperature dependence due to the presence of the thermal frequency $\Omega_{\rm th}$. In particular, we can consider the asymptotic limit of the high-temperature classical domain.

In the high-temperature classical domain dominated by thermal fluctuations, $(\Omega_{\rm th}/\omega) \gg 1$. In this limit,

$$\Phi\left(\mathrm{e}^{-\pi t\Omega_{\rm th}}, 1, \frac{\pm i\omega_c \pm \gamma + \pi}{\pi\Omega_{\rm th}}\right) \to \Phi(0, 1, \alpha) \to 0 \tag{31}$$

$$\coth\left(\frac{\omega_c \pm i\gamma}{\Omega_{\rm th}}\right) \to \frac{\Omega_{\rm th}}{\omega_c \pm i\gamma}. \tag{32}$$

Hence, the position–velocity correlation turns out to be

$$C_{xv_x}(t) = -\frac{k_B T}{m}\mathrm{e}^{-\gamma t}\left[\frac{\omega_c \sin(\omega_c t) - \gamma\cos(\omega_c t)}{\omega_c^2 + \gamma^2}\right]. \tag{33}$$

Setting the limits $t = 0$ and $\omega_c = 0$, we get the following expected result: $C_{xv_x}(0) = k_B T/m\gamma$.

4.2 *Drude model*

As in the case of the Ohmic model, in this case also one can write the expression for the position–velocity correlation function using eqs (16) and (27).

$$C_{xv_x}(t) = \frac{-i\hbar}{2\pi m}\int_{-\infty}^{\infty} \mathrm{d}\omega \left(\frac{\gamma}{1+\omega^2\tau^2}\right)\coth\left(\frac{\omega}{\Omega_{\rm th}}\right)\mathrm{e}^{-i\omega t} \times \frac{\left[\left(\omega + \frac{\omega\gamma\tau}{1+\omega^2\tau^2}\right)^2 + \omega_c^2 + \left(\frac{\gamma}{1+\omega^2\tau^2}\right)^2\right]}{\left\{\left[\left(\omega + \frac{\omega\gamma\tau}{1+\omega^2\tau^2}\right)^2 + \omega_c^2 + \left(\frac{\gamma}{1+\omega^2\tau^2}\right)^2\right]^2 - 4\omega_c^2\left(\omega + \frac{\omega\gamma\tau}{1+\omega^2\tau^2}\right)^2\right\}}. \tag{34}$$

In this case too, like the response function, we solve the integral numerically for both the high-temperature classical and low-temperature quantum regimes. Figures 2 and 3 show the time evolution of the position–velocity correlation function in the high-temperature domain and low-temperature domain, respectively. For both cases we have discussed the different regimes (underdamped, overdamped and critically damped) following the same parameters and notations used in figure 1.

5. Velocity autocorrelation function

5.1 *Ohmic model*

For the Ohmic model, the velocity autocorrelation function is given by

$$C_{v_x}(t) = \frac{\gamma\hbar}{2\pi m} \times \int_{-\infty}^{\infty} \frac{\omega(\omega^2 + \omega_c^2 + \gamma^2)\coth(\frac{\omega}{\Omega_{\rm th}})}{\left[(\omega^2 + \omega_c^2 + \gamma^2)^2 - 4\omega^2\omega_c^2\right]}\mathrm{e}^{-i\omega t}\mathrm{d}\omega. \tag{35}$$

The poles for the above expression are located at $\omega = -in\pi\Omega_{\rm th}$ and $\omega = (\omega_c + i\gamma)$, $(-\omega_c + i\gamma)$, $(\omega_c - i\gamma)$ and $(-\omega_c - i\gamma)$. Of these, only the poles at $-in\pi\Omega_{\rm th}$, $(\omega_c - i\gamma)$ and $(-\omega_c - i\gamma)$ lie within the lower contour. Thus, the above integration can be calculated using Cauchy's residue theorem and we get

$$\begin{aligned} C_{v_x}(t) = {} & \frac{-i\hbar}{4\pi m}\mathrm{e}^{-\pi t\Omega_{\rm th}} \\ & \times \Bigg\{(\omega_c + i\gamma)\left[\Phi\left(\mathrm{e}^{-\pi t\Omega_{\rm th}}, 1, 1 + \frac{-i\omega_c + \gamma}{\pi\Omega_{\rm th}}\right) + \Phi\left(\mathrm{e}^{-\pi t\Omega_{\rm th}}, 1, 1 + \frac{i\omega_c - \gamma}{\pi\Omega_{\rm th}}\right)\right] \\ & - (\omega_c - i\gamma)\left[\Phi\left(\mathrm{e}^{-\pi t\Omega_{\rm th}}, 1, 1 + \frac{i\omega_c + \gamma}{\pi\Omega_{\rm th}}\right) + \Phi\left(\mathrm{e}^{-\pi t\Omega_{\rm th}}, 1, 1 + \frac{-i\omega_c - \gamma}{\pi\Omega_{\rm th}}\right)\right]\Bigg\} \\ & + \frac{\hbar}{4m}\mathrm{e}^{-\gamma t}\left[(\omega_c + i\gamma)\coth\left(\frac{\omega_c + i\gamma}{\Omega_{\rm th}}\right)\mathrm{e}^{i\omega_c t}\right. \\ & \left. + (\omega_c - i\gamma)\coth\left(\frac{\omega_c - i\gamma}{\Omega_{\rm th}}\right)\mathrm{e}^{-i\omega_c t}\right]. \end{aligned} \tag{36}$$

In the high-temperature limit $((\Omega_{\rm th}/\omega) \gg 1)$, the velocity autocorrelation turns out to be

$$C_{v_x}(t) = \frac{k_B T}{m}\mathrm{e}^{-\gamma t}\cos(\omega_c t). \tag{37}$$

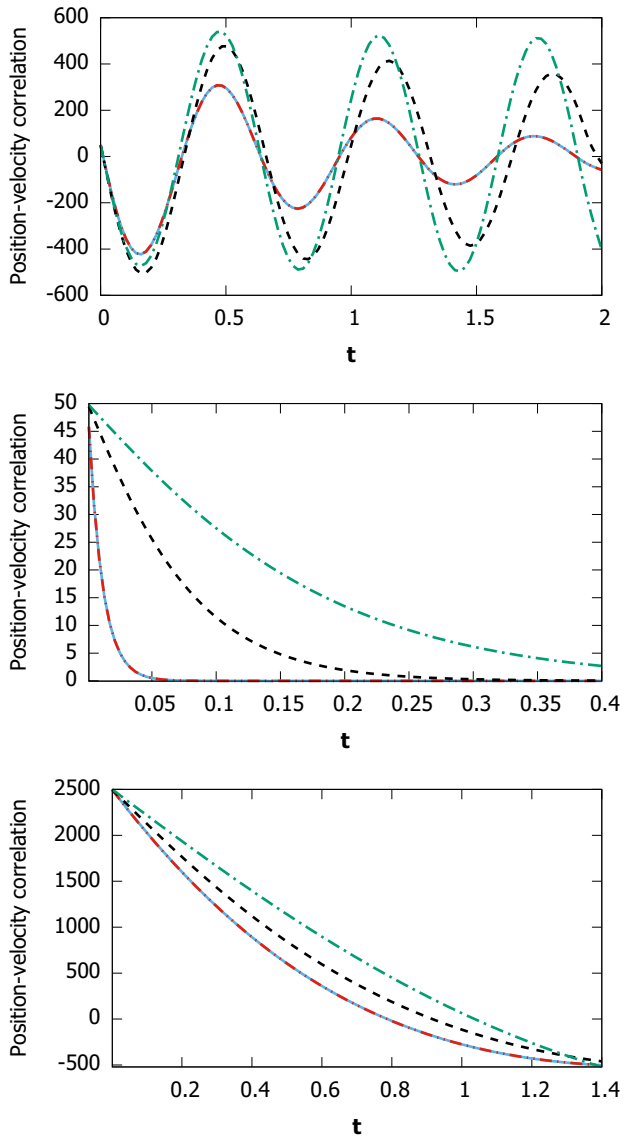

Figure 2. Time evolution of the position–velocity correlation function in the high-temperature domain, for $\Omega_{\text{th}} = 10^4$. (**Top**) The underdamped ($\omega_c = 10$, $\gamma = 1$), (**middle**) the overdamped ($\omega_c = 1$, $\gamma = 100$) and (**bottom**) the critically damped ($\omega_c = 1$, $\gamma = 1$) cases. In all the cases, the solid blue line is for the Ohmic case using eq. (29), the double dot-dash red line is for the Drude case $\tau = 0$, the dashed black line is for $\tau = 0.5$ and the dot-dash green line is for $\tau = 1$.

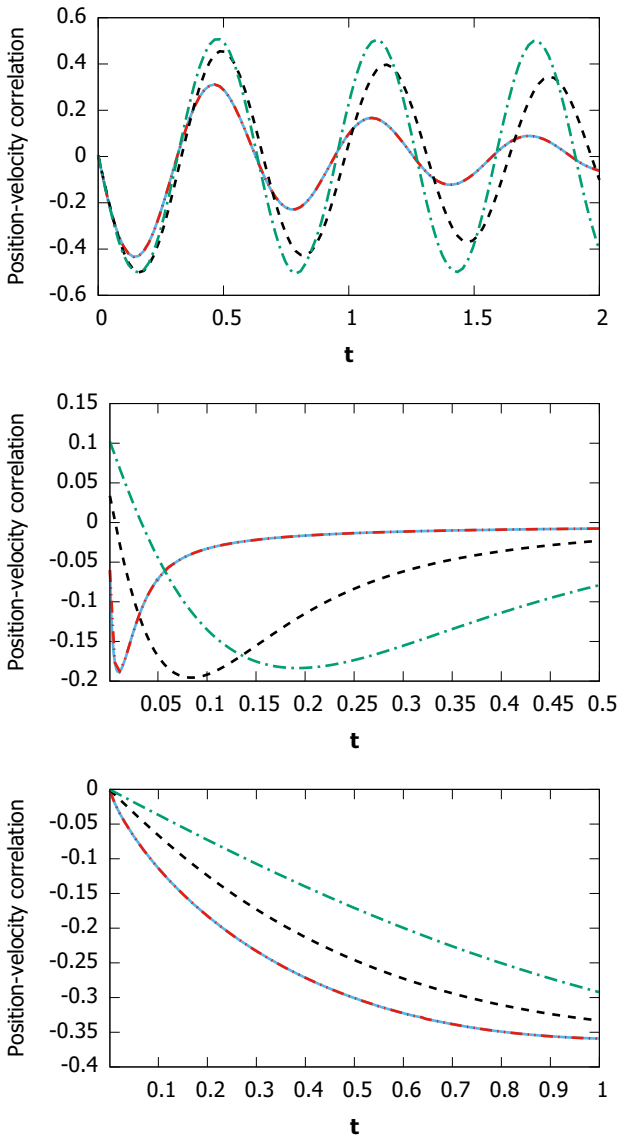

Figure 3. Time evolution of the position–velocity correlation function in the low-temperature domain for $\Omega_{\text{th}} = 0.1$. (**Top**) The underdamped ($\omega_c = 10$, $\gamma = 1$), (**middle**) the overdamped ($\omega_c = 1$, $\gamma = 100$) and (**bottom**) the critically damped ($\omega_c = 1$, $\gamma = 1$) cases. In all the cases, solid blue line is for the Ohmic case using eq. (29), the double dot-dash red line is for the Drude case $\tau = 0$, the dashed black line is for $\tau = 0.5$ and the dot-dash green line is for $\tau = 1$.

At $t = 0$, $C_{v_x}(0) = k_B T/m$, which is expected in the thermal fluctuation-dominated classical regime and is consistent with the Equipartition theorem.

5.2 *Drude model*

Using eqs (18) and (27), the velocity autocorrelation in this case is given by

$$C_{v_x}(t) = \frac{\hbar}{2\pi m}\int_{-\infty}^{\infty} \mathrm{d}\omega \left(\frac{\gamma\omega}{1+\omega^2\tau^2}\right) \frac{\left[\left(\omega + \frac{\omega\gamma\tau}{1+\omega^2\tau^2}\right)^2 + \omega_c^2 + \left(\frac{\gamma}{1+\omega^2\tau^2}\right)^2\right] \coth\left(\frac{\omega}{\Omega_{\text{th}}}\right) \mathrm{e}^{-i\omega t}}{\left\{\left[\left(\omega + \frac{\omega\gamma\tau}{1+\omega^2\tau^2}\right)^2 + \omega_c^2 + \left(\frac{\gamma}{1+\omega^2\tau^2}\right)^2\right]^2 - 4\omega_c^2\left(\omega + \frac{\omega\gamma\tau}{1+\omega^2\tau^2}\right)^2\right\}}. \tag{38}$$

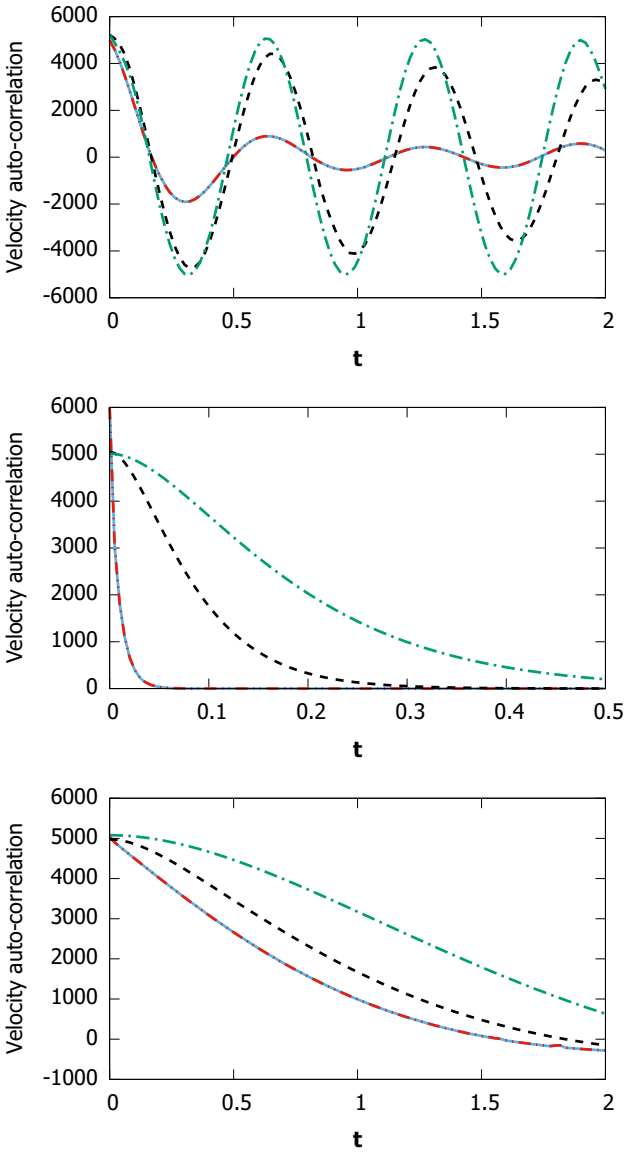

Figure 4. Time evolution of the velocity autocorrelation function in the high-temperature domain for $\Omega_{\rm th} = 10^4$. (**Top**) The underdamped ($\omega_c = 10$, $\gamma = 1$), (**middle**) the overdamped ($\omega_c = 1$, $\gamma = 100$) and (**bottom**) the critically damped ($\omega_c = 1$, $\gamma = 1$) cases. In all the cases, solid blue line is for the Ohmic case using eq. (36), the double dot-dash red line is for the Drude case $\tau = 0$, the dashed black line is for $\tau = 0.5$ and the dot-dash green line is for $\tau = 1$.

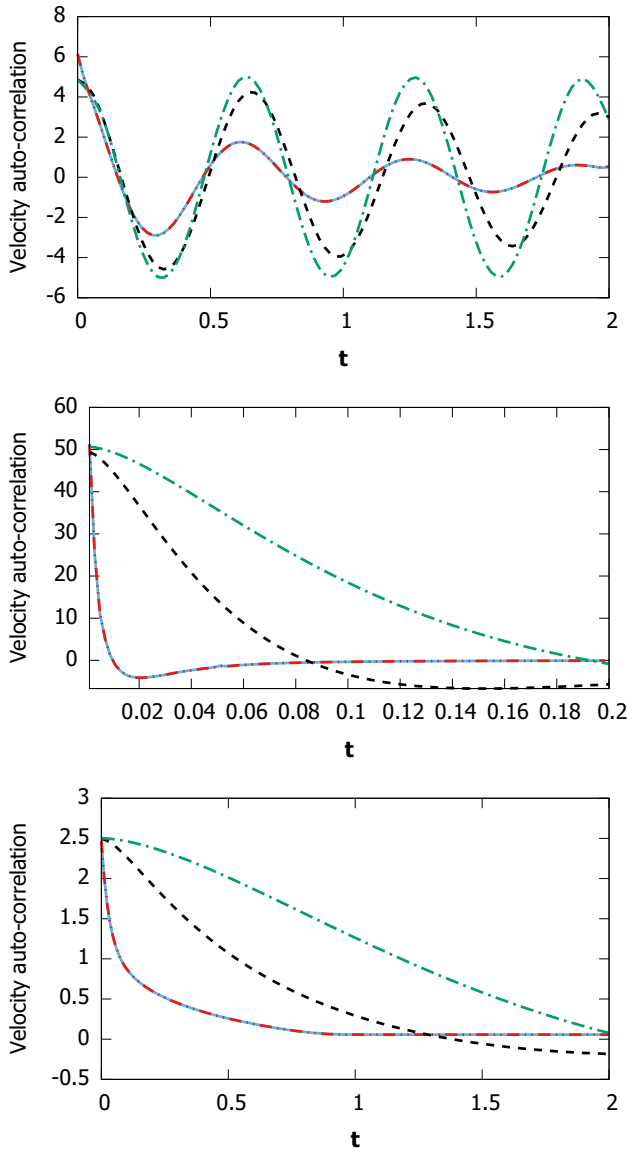

Figure 5. Time evolution of the velocity autocorrelation function in the low-temperature domain for $\Omega_{\rm th} = 0.1$. (**Top**) The underdamped ($\omega_c = 10$, $\gamma = 1$), (**middle**) the overdamped ($\omega_c = 1$, $\gamma = 100$) and (**bottom**) the critically damped ($\omega_c = 1$, $\gamma = 1$). In all the cases, the solid blue line is for the Ohmic case using eq. (36), double dot-dash red line is for the Drude case $\tau = 0$, the dashed black line is for $\tau = 0.5$ and the dot-dash green line is for $\tau = 1$.

We analyse this integral numerically like the other physical observables discussed in earlier sections, for the Drude model, for both the high-temperature ($(\Omega_{\rm th}/\omega) \gg 1$) and low-temperature ($(\Omega_{\rm th}/\omega) \ll 1$) regimes.

Figures 4 and 5 show the time evolution of the velocity autocorrelation function in the high-temperature domain and low-temperature domain respectively. For both cases, we have discussed the different regimes (underdamped, overdamped and critically damped) following the same parameters and notations used in figures 2 and 3.

6. Results: Comparison of Ohmic and Drude models

In this section we discuss the results displayed in figures 1–5.

In figure 1 we study the behaviour of the response function for the Ohmic and the Drude models for various values of τ, the memory time (the Drude time) in the underdamped ($\omega_c \gg \gamma$), overdamped ($\omega_c \ll \gamma$) and critically damped ($\omega_c = \gamma$) regimes. We have explicit analytical forms for the Ohmic model (eqs (24), (29) and (36)) which enables an easy comparison with the results obtained in the Ohmic limit ($\tau = 0$) for the Drude model. We notice that as τ goes up, the oscillations in the underdamped regime get to be more sustained. In the overdamped regime, for the Ohmic case, there is an initial steep rise in the response function before it settles down to the constant value of $1/m\gamma$ (see eq. (25)). This behaviour of the response function $R(t)$ of an initial increase followed by saturation to a fixed value determined by the viscous damping rate can be understood as follows: When we perturb a Brownian particle, it initially has a directional displacement before it gets completely randomised by a rate determined by the viscous damping rate. The overall trend is the same for the Drude model too. However, we notice that the Drude time-scale τ leads to a more sustained oscillation in the underdamped regime and leads to an effective slowing down of the damping in the overdamped regime. This can be understood as follows. The presence of memory, characterised by τ in the Drude model leads to a slowing down of the rise of the response function (as revealed in figure 1), which in turn means that randomising of the motion of the Brownian particle is slowed down leading to a weaker effect of dissipation on the particle. Since the damped harmonic oscillation is a consequence of a competition between the oscillatory effect of the cyclotron frequency and the damping effect of viscosity, it is clear that the presence of a finite τ results in more sustained oscillations than in the Ohmic case where $\tau = 0$. In the critically damped case, the behaviour of the response function is between the two extremes of underdamped and overdamped regimes.

Let us now discuss the position–velocity correlation function. We display a family of curves for various values of τ for the position–velocity correlation function in the high temperature regime for the overdamped, underdamped and critically damped cases in figure 2. We notice a transition from an oscillatory behaviour to an overdamped monotonic behaviour stemming from a competition between the oscillatory time-scale set by the cyclotron frequency ω_c and the damping rate γ. Such a transition from an oscillatory to a damped monotonic behaviour has been noticed in some earlier works in the context of damping of Bloch oscillations in optical lattices [3]. However, in ref. [3] the origin of these damped harmonic oscillations is quite distinct from the context dealt in this paper. Kolovsky *et al* [3] studied Bloch oscillations of cold neutral atoms in an optical lattice. Spontaneous emission causes the decay of Bloch oscillations, the decay rate being set by the rate of spontaneous emission. Furthermore, from our results, we notice that similar to the case of response function, in the under-damped regime, the increase in the memory time-scale leads to more sustained oscillations. In addition, in the overdamped and critically damped regime, the damping is slower for larger memory scales as seen in figure 2.

As in the high-temperature domain, we find that even in the low-temperature domain the position–velocity correlation function exhibits oscillations in the underdamped regime (figure 3). What is somewhat surprising is the presence of a non-monotonic trend in the position–velocity function in the overdamped regime at low temperatures. This is true for both the Drude case and the Ohmic case ($\tau = 0$) limit. This can be explained by the fact that noise correlations are inherently non-trivial (non-Markovian) in the low-temperature quantum domain. This is, perhaps, the origin of sustained memory-induced non-monotonic trends in the curves in the low-temperature overdamped regime. The position–velocity correlation goes towards negative values in the beginning and then turns around and finally tends to zero at large times. The time at which this turnaround takes place is dependent on the memory time τ and shifts towards larger values of time as τ increases. It is interesting to note that there has been a similar observation of sustained oscillations in the context of a classical Langevin equation (valid in the high-temperature domain) of a charged particle in a magnetic field for a Drude model in the presence of exponentially correlated noise [6]. Non-trivial noise correlation is a common feature in these two disparate cases (a classical Langevin dynamics of a charged particle in a magnetic field with correlated noise [6] and a quantum Langevin dynamics of a charged particle in a magnetic field with non-trivial quantum correlated noise, dealt with in this paper). Notice that in our analysis in the high-temperature limit of $(\Omega_{\rm th}/\omega) \gg 1$, such non-trivial noise correlations are absent, simply because one has a memory-free delta-correlated noise in that limit and thus we obtain a monotonic behaviour starting from a large positive value of the position–velocity correlation function which gets damped and goes over to zero in the long time limit.

The trends followed by the velocity autocorrelation function in various time–temperature regimes (figures 4 and 5) are similar to that of the position–velocity autocorrelation function. However, the non-monotonic feature discussed in the low-temperature, overdamped regime is less pronounced in the case of the velocity

autocorrelation function than in the case of the position–velocity correlation function.

7. Experimental implications

In recent experiments, correlation functions have been studied using a variety of methods. Many of these experiments measure the properties of the anomalous diffusion of cold atoms in optical lattices [18–20]. The experimental technique involved in ref. [21] uses optical tweezers for trapping the particles and the position correlations of the particles are measured using a high-bandwidth photodetector. In ref. [22], the position–velocity correlation function has been studied for ultracold Rb atomic cloud undergoing anomalous diffusion. The position–velocity correlation is then measured using a tomographic method which is a combination of absorption imaging and Raman velocity selection. In a recent paper [23], the measurement of the response function of ultracold Rb atomic cloud in a magneto-optical trap (MOT) and the spatial diffusion of the cloud in the absence of the MOT have been presented and analysed. As we know from the linear response theory, the response function is a measure of how a system responds to an external drive. In [23], a pulsed homogeneous magnetic field is used as an external driving force for measuring the response function. The atomic cloud gets displaced due to the external drive. Then it is allowed to equilibrate for some time and then finally returns to its original position when the external drive is turned off. The position of the cold atomic cloud is recorded at regular intervals after turning off the external drive and thus the path of the cloud is traced. In the same experiment, spatial diffusion of the atomic cloud is measured in the viscous medium provided by optical molasses. In this case, the MOT is turned off and the atomic cloud is allowed to diffuse in the presence of optical molasses and the mean square displacement (the position correlation function) is measured using an absorption imaging technique. As discussed in §2, a knowledge of the position autocorrelation enables us to compute the position–velocity and velocity autocorrelation functions. These predictions can be tested using the techniques in ref. [23] with hybrid traps for ions and neutral atoms, and additionally a uniform magnetic field can be provided using a combination of Helmholtz configuration magnetic coils.

8. Concluding remarks

In this paper, we studied the interplay between the cyclotron frequency and the viscous damping rate via the quantum Langevin equation for a charged particle coupled to a bath in the presence of a magnetic field. In particular, we studied the response function, the position–velocity correlation function and the velocity autocorrelation for two bath models – the Ohmic bath and the Drude bath models and made a detailed comparison in various time–temperature regimes. It is pertinent to mention here that, to our knowledge, such a detailed investigation has not been done earlier. To be more specific, our results of position–velocity correlation are of extreme importance, as it has been rarely studied analytically in literature, in spite of having experimental importance [22].

In the zero-point fluctuation-dominated low-temperature regime, non-trivial noise correlations lead to some interesting features in the transition from an oscillatory to a monotonic behaviour. We also studied the role of the memory time-scale which comes into play in the Drude model and investigated the effect of this additional time-scale. We thus saw a rich interplay of various time-scales set by the cyclotron frequency ω_c, the damping rate γ, the Drude time-scale τ and the thermal time-scale $\beta\hbar$ which controls the noise correlations in the quantum domain. Our study is unique in addressing the richness of all these time-scales, sweeping across the thermal fluctuation-dominated classical regime and the quantum fluctuation-dominated quantum regime. We are not aware of such a comprehensive study of the response function, the position–velocity correlation function and the velocity autocorrelation function for a charged particle in a magnetic field in a viscous medium.

In refs [24–28], a power law decay ($t^{-\alpha}$) of the velocity autocorrelation function has been observed at long times, with $\alpha = 3/2$ in the classical regime and $\alpha = 2$ for position correlation in the quantum regime. In our study too we noticed a slow long-time decaying behaviour (figures 4 and 5) of the correlation functions at overdamped and critically damped regimes, both in the classical and quantum domains. The precise nature of the long time tails lies outside the scope of the present study and can be analysed in detail in the future.

In this paper, we considered a QLE of a charged quantum Brownian particle in the presence of a magnetic field and linearly coupled via position coordinate to a bath. In contrast, in ref. [29], Gupta and Bandyopadhyay derived a QLE for a charged quantum particle in a harmonic potential in the presence of a uniform external magnetic field and coupled linearly through the momentum variables to a bath of oscillators. In that context, they noticed that the magnetic field appears through a quantum generalised classical Lorentz force term. In addition, the QLE involves a random force independent of the magnetic field. While these aspects are also there in the present analysis of the QLE for a charged quantum Brownian

particle coupled to the bath via position coordinate [9], there are significant differences: (i) The random force has a modified form with symmetric correlation and unequal time commutator different from those in the case of coordinate–coordinate coupling, (ii) the inertial term and the harmonic potential term in the QLE get renormalised as a consequence of the renormalisation of the mass and (iii) the memory function characterising the mean force in the QLE not only has a magnetic field-independent diagonal part, but also an explicit magnetic field-dependent off-diagonal part [29]. We therefore expect the behaviour of the various correlation functions analysed and depicted here to get qualitatively and quantitatively modified in the context of a momentum coupling between the charged particle and the bath.

We expect our work to generate interest among experimentalists to test the predictions that stem out of our theoretical study.

References

[1] R Balescu, *Equilibrium and non-equilibrium statistical mechanics* (John Wiley & Sons, 1975)

[2] G F Mazenko, *Non-equilibrium statistical mechanics* (Wiley-VCH Verlag GmbH & Co. KGaA, 2006)

[3] A R Kolovsky, A V Ponomarev and H J Korsch, *Phys. Rev. A* **66**, 053405 (2002)

[4] M B Dahan, E Peik, J Reichel, Y Castin and C Salomon, *Phys. Rev. Lett.* **76**, 4508 (1996)

[5] A Einstein, *Ann. Phys.* **322**(**8**), 549 (1905)

[6] N Francis, C Paraan, M P Solon and J P Esguerra, *Phys. Rev. E* **77**, 022101 (2008)

[7] S Dattagupta and J Singh, *Pramana – J. Phys*. **47**, 211 (1996)

[8] X L Li, G W Ford and R F O'Connell, *Phys. Rev. A* **41**, 5287 (1990)

[9] X L Li, G W Ford and R F O'Connell, *Phys. Rev. A* **42**, 4519 (1990)

[10] U Weiss, *Quantum dissipative systems*, 4th edition (2012)

[11] G W Ford, M Kac and P Mazur, *J. Math. Phys.* **6**(**4**), 504 (1965)

[12] U Satpathi and S Sinha, *Phys. A Stat. Mech. Appl.* **506**, 692 (2018)

[13] G W Ford, J T Lewis and R F O'Connell, *Phys. Rev. A* **37**, 4419 (1988)

[14] P Hänggi and G L Ingold, *Chaos* **15**(**2**), 026105 (2005)

[15] C F Bohren, *Eur. J. Phys.* **31**(**3**), 573 (2010)

[16] G W Ford and R F O'Connell, *Phy. Rev. D* **64**(**10**), 105020 (2001)

[17] A Das, A Dhar, I Santra, U Satpathi and S Sinha, *Phys. Rev. E* **102**, 062130 (2020)

[18] E Barkai, E Aghion and D A Kessler, *Phys. Rev. X* **4**, 021036 (2014)

[19] H Katori, S Schlipf and H Walther, *Phys. Rev. Lett.* **79**, 2221 (1997)

[20] Y Sagi, M Brook, I Almog and N Davidson, *Phys. Rev. Lett.* **108**, 093002 (2012)

[21] M Grimm, T Franosch and S Jeney, *Phys. Rev. E* **86**, 021912 (2012)

[22] G Afek, J Coslovsky, A Courvoisier, O Livneh and N Davidson, *Phys. Rev. Lett.* **119**, 060602 (2017)

[23] S Bhar, M Swar, U Satpathi, S Sinha, R D Sorkin, S Chaudhuri and S Roy, *Measurements and analysis of response function of cold atoms in optical molasses*, arXiv: 2101.09118 (2021)

[24] G L Paul and P N Pusey, *J. Phys. A Math. Gen.* **14**(**12**), 3301 (1981)

[25] B U Felderhof, *J. Phys. Chem. B* **109**(**45**), 21406 (2005)

[26] C Aslangul, N Pottier and D Saint-James, *J. Stat. Phys.* **40**, 167 (1985)

[27] N Pottier and A Mauger, *Phys. A Stat. Mech. Appl.* **282**(**1**), 77 (2000)

[28] R Jung, G L Ingold and H Grabert, *Phys. Rev. A* **32**, 2510 (1985)

[29] S Gupta and M Bandyopadhyay, *Phys. Rev. E* **84**, 041133 (2011)